J Seismol (2008) 12:453–475
DOI 10.1007/s10950-008-9098-y

ORIGINAL ARTICLE

Broadband (0.05 to 20 s) prediction of displacement response spectra based on worldwide digital records

Carlo Cauzzi · Ezio Faccioli

Received: 6 December 2007 / Accepted: 3 March 2008 / Published online: 29 April 2008

Abstract A new set of empirical equations for prediction of displacement response spectral ordinates from 20 Hz to T=20 s is illustrated. The coefficients of the equations were obtained by regressing a dataset based on 1,155 tri-axial digital and 9 analog accelerometer records from 60 earthquakes worldwide. Long period disturbances in the accelerograms were evaluated and removed using a very recent method, aimed at preserving the long-period spectral content of the records. Analysis of variance has disclosed only little evidence for regional dependence of ground motions, while a carefully conducted evaluation of site effects resulted in clearly differentiated spectral amplification bands associated to the main ground types B, C, and D of Eurocode 8. Spectral ordinates for vibration periods >5 s were found to scale with magnitude quite consistently with theoretical scaling from Brune's model. On the other hand, comparison of results with those yielded by recent prediction models in Europe and the United States (NGA), indicated that the latter may not be uniformly reliable at long periods. The proposed empirical equations are easily implemented in computer programs for seismic hazard assessment, being characterized by a simple functional form and a restricted number of predictor variables.

Keywords Attenuation relationships · Digital accelerograms · Displacement-based design · Displacement response spectra · Ground motion prediction · Long-period ground motion

1 Introduction

Following the developments of the last 10 years, which placed strong emphasis on displacement considerations and *capacity design* concepts (Park and Paulay 1976), the earthquake resistant design of structures has increasingly become *performance-based*. In this process, the primary descriptor of the seismic demand becomes the relative displacement of the structure caused by the imposed ground motion, quantified through the displacement response spectrum (hereafter DRS). In particular, among the different methods for *displacement-based* design proposed in recent years, the direct displacement-based design approach (Priestley et al. 2007) replaces the actual structure (a nonlinear multi-*dof* system) with an equivalent linear 1 *dof* system, in which energy dissipation due to nonlinear response is

Electronic supplementary material The online version of this article (doi:10.1007/s10950-008-9098-y) contains supplementary material, which is available to authorized users.

C. Cauzzi (✉) · E. Faccioli
Department of Structural Engineering,
Politecnico di Milano,
Piazza Leonardo da Vinci, 32,
20133 Milan, Italy
e-mail: cauzzi@stru.polimi.it

E. Faccioli
e-mail: faccioli@stru.polimi.it

accounted for through a large (up to 30%) equivalent viscous damping factor. As design involves the response of the damaged structure, equivalent linearization may require the determination of displacement response spectral ordinates at periods well beyond the typical 0- to 4-s range of current norms like Eurocode 8 (CEN 2004). At such long periods, the lack of accuracy of traditional strong motion data has long been considered as a major limitation to determine reliable displacement spectra.

The foregoing recent advances in the design of structures stimulated, in Italy, a national research project called S5 (Internet site: progettos5.stru.polimi.it), sponsored by the Department of Civil Defence, initiated in mid-2005 and concluded in July 2007. The project aimed at providing a model of the seismic action in terms of arbitrarily damped DRS, extending to long periods and suitable for introduction in seismic codes, as well as national hazard maps displaying the DRS values needed for design. The experience gained in previous studies on DRS at long periods (Faccioli et al. 2004) indicated at an early stage that crucial for the entire project was a tool for making reliable empirical predictions of horizontal and vertical, arbitrarily damped DRS, at periods from less than 1 s to more than 10 s.

Existing empirical equations for the prediction of spectral ordinates typically used for European regions either do not cover the entire period range of interest (e.g., Ambraseys et al. 2005, and Akkar and Bommer 2007a, among the most recent studies) or were found not to be sufficiently reliable at long periods (e.g., Berge-Thierry et al. 2003). This was mainly due to the restrictions imposed on the maximum allowable vibration period by high-pass filtering of the analog accelerograph recordings that make up most of the data sets of reference. Similar limitations also affect the Next Generation Attenuation (NGA) models (PEER 2007) developed in the United States, and their effect is well documented by Boore and Atkinson (2007, in press). These authors show that the potential number of records suitable for developing their prediction equations significantly decreases at periods $T>3$ s, even considering digital data only.

With this background, we illustrate herein a new set of empirical prediction equations for DRS ordinates, aimed at overcoming the previous restrictions. For this purpose, a new, worldwide database was assembled consisting almost exclusively of digitally recorded accelerograms of shallow crustal earthquakes, carefully selected in terms of ground type at the accelerograph sites, minimal long period disturbances in the record, and fullest possible coverage in the required magnitude and distance ranges, in view of the application to Italy (and Southern Europe). The following Section is devoted to the description of the worldwide database, while the predictive equations derived are presented in Section 3, and comparisons with other recent studies are provided in Section 4.

2 Worldwide digital database

The need of reliable empirical prediction equations for DRS over a very broad period range (>10 s), made us naturally opt for a reference dataset consisting exclusively of digital records. As a matter of fact, DRS computed from digital accelerograms depend only weakly on the adopted baseline correction procedures, as shown for example by Boore (2001) and Boore et al. (2002), and recent studies showed that records from colocated accelerometers and one-sample-per-second GPS exhibit a remarkable agreement of ground motions at periods up to and exceeding 30 s (Wang et al. 2007). The recent and innovative work by Paolucci et al. (2008), has made use of records from colocated broadband and digital strong motion instruments to show that response spectra from digital records are reliable up to periods much longer than usually thought, and that the displacement waveforms obtained by double integration of the accelerogram need not be free of unrealistic baseline drift if the objective is to obtain reliable spectral ordinates up to at least 10 s. Evidence of accelerometer and broadband instruments giving similar displacement traces was provided also by Jousset and Douglas (2007), though they used records from instruments which are closely located (distance <1 km), and not actually colocated as in Paolucci et al. (cit.). According to the latter authors, a noise index I_V can be defined and easily computed for each digital accelerogram, as a function of the maximum ground velocity and the average value computed on the *coda* of the velocity time history. Such noise index can be further compared with curves $I_V=I_V$ $(M_W;P)$ representing, as a function of magnitude M_W, the I_V values associated to a given probability P of the long period errors in the DRS to be less than a chosen threshold,

e.g., 15%. We retained in our dataset only those spectra having a probability $P \geq 0.9$ of the long period DRS drifts to be less than 15%. The I_V of the horizontal ground motion has been computed as the geometric mean of the I_V values of the two horizontal components.

Another important requirement imposed on the data was the availability of the shear wave velocity, V_S, profile as a basis for determining the local ground conditions at the recording sites: a substantial effort was made to reliably classify the majority of stations in the database according to the four main Eurocode 8 (EC8) ground categories, though few stations with unknown site conditions were retained in the dataset, as documented in Subsection 2.4.

The restrictions on the magnitude, depth, and distance ranges will be described in detail in Subsections 2.2 and 2.3.

2.1 Sources and regional distribution of data

The key resource for assembling the database were the data from the Japanese K-Net strong motion network (www.k-net.bosai.go.jp) because of the high quality of the available accelerograms and the detailed information provided for each recording site. This has made K-Net the largest contributing source to the dataset (82.5%), while the rest of accelerograms are from California, Europe, Iran, and Turkey. We looked for the most uniform possible coverage of the data space in terms of the main predictor variables of DRS, i.e., magnitude and distance. Thus, non-Japanese data were mainly used to cover those magnitude and distance intervals where the K-Net data available were not considered sufficient. Additional data from Japan included a set of records from the 1995 Hyogo-ken Nanbu earthquake, made available at the time of the Simultaneous Simulation Experiment of the 2nd International Symposium on ESG, in 1998 (JWGESG 1998), and ten records at rock sites from the Kik-Net network database (www.kik.bosai.go.jp). The Iran data were taken from the Iran Strong Motion Network, ISMN (www.bhrc.ac.ir/ISMN/Index.htm), while for California earthquakes, we mainly used data available from the USGS National Strong-Motion Program, NSMP (nsmp.wr.usgs.gov) and, for the 1999 Hector Mine event, digital data from the Engineering Strong Motion Data Center, CISN (www.quake.ca.gov/cisn-edc) and from the Southern California Seismic Network, SCSN (www.scsn.org). Concerning Europe and Turkey, nearly all of the selected records were digitally recorded accelerograms from the strong-motion data archive at the Imperial College of London (Ambraseys et al. 2002). All data were entered in the database in the form of uncorrected acceleration time histories, with the exception of nine accelerograms of the 1980 Irpinia (Italy) M_W 6.9 earthquake (also available in the Imperial College of London database); these are the only analog recordings present in the database and were introduced in it only after a careful scrutiny of their long period characteristics. The final dataset consists of 1,164 accelerograms (from 60 earthquakes), of which 84% is from Japan, 6% is from Iran, 5% is from the United States, and 5% is from Europe and Turkey. The details of this dataset can be obtained from the authors; it is the final result of a long selection and assembling process (see Faccioli et al. 2007 and Paolucci et al. 2008 for information on previous versions).

2.2 Magnitude, depth, and focal mechanism

We looked for crustal earthquakes worldwide with independently determined moment magnitude, in the $5.0 \leq M_W \leq 7.2$ range. The lower magnitude bound was dictated by the results of probabilistic deaggregation analyses of seismic hazard at many sites in Italy, showing that contributions of the $M_W < 5+$ events to spectral displacement hazard are very low or negligible (see, e.g., Fig. 4). On the other hand, the upper bound is representative of the largest estimated magnitudes in the historical earthquakes catalog in Italy (Gruppo di Lavoro CPTI 2004). The chosen magnitude range is believed to be more generally representative for crustal earthquakes of Southern Europe including the Balkan region. M_W values of Japanese events, representing the majority of the dataset, were taken from the F-Net broadband network (www.fnet.bosai.go.jp/freesia/index-j.html), while most of those of the other events were from the Harvard global CMT catalog (www.globalcmt.org/CMTsearch.html). The magnitudes of the selected crustal earthquakes from Japan do not exceed 6.8, so that all the $M_W > 6.8$ events in the dataset are from Europe, the Middle East, Iran, and California. The upper magnitude bound adopted has led to rejecting extensively recorded events such as the 1999 (M_W

7.6) Chi-Chi mainshock which is, on the contrary, the main data source in the database of Boore and Atkinson (2007, in press) within the NGA project (PEER 2007). The CMT moment magnitude was used for Japanese earthquakes occurring before 1997, as moment tensor solutions are not available from F-Net.

Subduction zone events were excluded from the database, and focal depths were restricted within about 22 km, which is also consistent with the largest "effective depth" class of 12–20 km in the Italian Seismic Source Zones (SSZ) model. For Japanese earthquakes, the K-Net focal depths were chosen, after checking for a number of events that these coincide with those reported in the Hi-Net database (www.hinet.bosai.go.jp), while most of focal depths of the other events were taken from the cited CMT catalogue.

As to the focal mechanisms, a classification scheme based on the plunges of the *P*-, *T*-, and *B*-axes was adopted, following Boore and Atkinson (cit.). As underlined in Stafford et al. (2008), the classification scheme by Boore and Atkinson (cit.) is consistent with that used for European earthquakes by Ambraseys et al. (2005) and Akkar and Bommer (2007a, b). The plunges of the *P*- and *T*-axes were derived for all the events of the present database, using as main sources the Harvard global CMT catalogue and the F-Net moment tensor database. No undefined mechanism was found in the present dataset of 60 earthquakes, which contains 32 strike-slip (M_W range 5–7.2), 16 normal fault (M_W range 5–6.9), and 12 reverse fault events (M_W range 5.3–6.6). The moment magnitude, depth, and style-of-faulting of each earthquake are listed in Table 1.

2.3 Distance

The focal distance, *R*, was chosen, mainly for greater flexibility of usage in seismic hazard analyses contemplating SSZs of variable depth, as is the case in Italy, where an "effective" focal depth is associated to each source zone (see zonesismiche.mi.ingv.it/documenti/App2.pdf). The distance limit of 150 km was dictated by the deaggregation analyses mentioned in Subsection 2.2. The smallest value of *R* in the dataset is about 6 km.

While the use of distance to the fault rupture, in preference to the focal distance, will be further investigated in future work on the present data, a first step in this direction has been taken by deriving a correlation between focal (R) and fault (R_f) distances on the basis of a subset of nine earthquakes with well-defined source geometry and $M_W \geq 6.0$. The obtained relationship is

$$R(\mathrm{km}) = 10.7 + 0.99 R_f(\mathrm{km}) \quad (\sigma_R = 6.37; r^2 = 0.97). \tag{1}$$

The distribution of the acceleration records in the database is depicted in Fig. 1, with respect to magnitude, distance, and geographical origin of data.

2.4 Site conditions

As previously mentioned, the four basic ground categories (A, B, C, and D, with the following V_{S30} values, respectively: $V_{S30} \geq 800$ ms^{-1}; 360 ms$^{-1} \leq V_{S30} < 800$ ms^{-1}; 180 ms$^{-1} \leq V_{S30} < 360$ ms^{-1}, and $V_{S30} < 180$ ms^{-1}) contemplated in the current European (CEN 2004) seismic codes, have been adopted for the classification of the recording sites.

For the recording sites in the K-Net database, the profile of P and S wave velocities at the recording sites extends to a maximum depth of 20 m. The methods we adopted to estimate V_{S30} from velocity data not reaching 30 m depth are described in Faccioli et al. (2007), based on the work by Figini (2006), who used three methods suggested by Boore (2004) and developed an independent additional one. The simplest method taken from Boore (cit.) assumes that the lowermost measured velocity extends down to 30 m, but this choice may lead to underestimating V_{S30} because V_S generally increases with depth in layered soil profiles. To overcome this problem, the criterion was modified by assuming piecewise uniform velocity profiles: specifically, the deepest measured velocity value was increased by 20% every 10 m. Two more options were borrowed from Boore (cit.): the first is based on velocity statistics to determine the site class, while the second one uses the correlation between V_{S30} and V_{Sd}, where V_{Sd} is the time-averaged velocity for a set of boreholes for which the actual depth d reaches or exceeds 30 m. The correlation between V_{S30} and V_{Sd} was calibrated ad hoc for this study using about 100 velocity profiles from the Kik-Net database (Figini, cit.). The actual classification of the K-Net stations was finally established by applying the four criteria just described, and the final decision

Table 1 Earthquakes in the reference database

Earthquake date and time (UT)	Epicentral area (country, number of records)	Earthquake mechanism	Depth (km)	M_W
1995_January_16_20:46	Hyogo-Ken Nanbu (J, 6)	Strike-slip	17.9[a]	6.9[b]
1996_August_10_18:12	Honshu (J, 27)	Reverse	7[c]	5.9[b]
1996_August_10_23:10	Honshu (J, 27)	Strike-slip	10[c]	5.7[b]
1996_September_09_04:34	Kyushu (J, 10)	Normal	20[c]	5.7[b]
1997_March_04_03:51	Central Izu Peninsula (J, 24)	Strike-slip	2[c]	5.5[d]
1997_March_26_08:31	NW Kagoshima Prefecture (J, 63)	Strike-slip	8[c]	6.1[d]
1997_April_02_19:33	NW Kagoshima Prefecture (J, 43)	Strike-slip	9[c]	5.4[d]
1997_May_13_05:38	NW Kagoshima Prefecture (J, 68)	Strike-slip	8[c]	6[d]
1997_June_25_09:50	Yamaguchi Prefecture (J, 38)	Strike-slip	12[c]	5.8[d]
1998_May_03_02:09	E Off Izu Peninsula (J, 23)	Strike-slip	3[c]	5.5[d]
1998_August_15_18:31	Hida Mountains (J, 38)	Strike-slip	5[c]	5.3[d]
1998_September_03_07:58	N Iwate Prefecture (J, 20)	Reverse	10[c]	5.9[d]
2000_June_06_21:16	Nw Off Hokuriku District (J, 15)	Reverse	22[c]	5.8[d]
2000_June_29_06:30	Near Miyakejima Island (J, 8)	Strike-slip	20[c]	5.6[d]
2000_July_01_07:02	Near Niijima Island (J, 24)	Normal	15[c]	6.2[d]
2000_July_02_20:03	Near Miyakejima Island (J, 16)	Normal	18[c]	5.6[d]
2000_July_08_18:57	Near Miyakejima Island (J, 10)	Normal	14[c]	5.9[d]
2000_July_15_01:30	Near Niijima Island (J, 33)	Strike-slip	5[c]	6[d]
2000_July_23_21:52	Near Niijima Island (J, 7)	Normal	9[c]	5.6[d]
2000_July_27_01:49	Near Miyakejima Island (J, 7)	Strike-slip	12[c]	5.5[d]
2000_July_30_00:18	Near Miyakejima Island (J, 4)	Strike-slip	14[c]	5.7[d]
2000_July_30_12:25	Near Miyakejima Island (J, 10)	Strike-slip	18[c]	6.4[d]
2000_July_30_12:49	Near Miyakejima Island (J, 6)	Strike-slip	18[c]	5.6[d]
2000_August_03_13:18	Near Niijima Island (J, 7)	Normal	12[c]	5.2[d]
2000_August_18_01:52	Near Niijima Island (J, 7)	Strike-slip	11[c]	5.7[d]
2000_October_06_04:30	W Tottori Prefecture (J, 44)	Strike-slip	11[c]	6.6[d]
2000_October_08_04:17	Shimane Hiroshima Border (J, 53)	Strike-slip	8[c]	5.1[d]
2001_December_18_04:02	Near Ishigakijima Island(J, 2)	Normal	12[c]	6.8[d]
2002_January_12_00:18	NW Off Miyakojima Island (J, 1)	Normal	5[d]	5.2[d]
2002_April_28_13:23	NW Off Ishigakijima Island (J, 1)	Normal	16[c]	5[d]
2003_July_25_15:13	N Miyagi Prefecture (J, 15)	Reverse	12[c]	5.5[d]
2003_July_25_22:13	N Miyagi Prefecture (J, 47)	Reverse	12[c]	6.1[d]
2003_July_26_07:56	N Miyagi Prefecture (J, 46)	Reverse	12[c]	5.3[d]
2004_October_23_08:56	Mid Niigata Prefecture (J, 47)	Reverse	13[c]	6.6[d]
2004_October_23_09:34	Mid Niigata Prefecture (J, 43)	Reverse	14[c]	6.3[d]
2004_December_14_05:56	Rumoi (J, 29)	Reverse	9[c]	5.7[d]
2005_March_20_01:53	NW Off Kyushu (J, 40)	Strike-slip	9[c]	6.6[d]
2005_March_22_06:55	NW Off Kyushu (J, 2)	Strike-slip	11[c]	5[d]
2005_April_19_21:11	NE Fukuoka Prefecture (J, 65)	Strike-slip	14[c]	5.4[d]
1997_February_04_10:37	Garmkhan (I, 3)	Strike-slip	15[b]	6.5[b]
1997_May_10_07:57	Ardakul (I, 4)	Strike-slip	15[b]	7.2[b]
1999_May_06_23:00	Karehbas (I, 14)	Strike-slip	17.4[b]	6.2[b]
2002_June_22_02:58	Changureh-Avaj (I, 35)	Reverse	15[b]	6.5[b]
2003_December_26_01:56	Bam (I, 1)	Strike-slip	15[b]	6.6[b]
2005_February_22_02:25	Zarand (I, 12)	Reverse	12[b]	6.4[b]
1999_October_16_09:46	Hector Mine (C, 26)	Strike-slip	15[b]	7.1[b]
2000_September_03_08:36	Yountville (C, 18)	Strike-slip	9.4[e]	5[e]
2003_December_22_19:15	San Simeon (C, 3)	Reverse	7.6[e]	6.4[e]
2005_June_12_15:41	Anza (C, 12)	Strike-slip	14.1[e]	5.2[e]
1999_August_19_15:17	Izmit (T, 1)	Normal	12[f]	5.1[b,f]
1999_August_31_08:10	Izmit (T, 9)	Normal	4[f]	5.2[f]
1999_November_12_16:57	Duzce (T, 8)	Strike-slip	14[f]	7.2[f]

Table 1 (continued)

Earthquake date and time (UT)	Epicentral area (country, number of records)	Earthquake mechanism	Depth (km)	M_W
2003_May_01_00:27	Bingol (T, 1)	Strike-slip	10[f]	6.3[b,f]
2000_June_17_15:40	South Iceland (IC, 10)	Strike-slip	15[b,f]	6.5[b,f]
2000_June_21_00:51	South Iceland (IC, 10)	Strike-slip	15[b,f]	6.4[b,f]
1980_November_23_18:34	Irpinia (IT, 9)	Normal	16[f]	6.9[b,f]
1997_October_06_23:24	Umbria-Marche (IT, 2)	Normal	7[f]	5.5[b,f]
1997_October_12_11:08	Umbria-Marche (IT, 4)	Normal	6[f]	5.2[b,f]
1997_October_14_15:23	Umbria-Marche (IT, 4)	Normal	7[f]	5.6[f]
1998_April_03_07:26	Umbria-Marche (IT, 2)	Normal	6[f]	5.1[b,f]

Geographical origin of data shown in column 2: Japan (J), Iran (I), California (C), Turkey (T), Iceland (IC), and Italy (IT)
[a] ESG98
[b] Harvard Global CMT
[c] K-Net
[d] F-Net
[e] USGS
[f] ESMD

on the ground category was taken on a simple majority rule.

The site conditions at European and Turkish stations were classified mainly using the information available in the European Strong-Motion database (Ambraseys et al. 2002) and in Rey et al. (2002); however, we independently checked the attributed ground category for a number of Turkish and Icelandic stations, on the basis of recently published studies (e.g., Rathje et al. 2006; Halldórsson et al. 2007). Ground conditions for Iran records were identified, where possible, starting from the classification scheme proposed by Zaré (2004). Finally, for California data, qualitative information on ground conditions is available for CISN network stations, while many NSMP stations were classified using online data available from David M. Boore's home page (Internet site: quake.wr.usgs.gov/~boore), Boore et al. (1997), and a few USGS open-file reports.

The distribution of records in terms of magnitude, focal distance, and ground category is shown in Fig. 2a: stations on ground type A are 6% of the whole database, those on type B sites are 43%, on type C 38%, and on type D 9%. The remaining 4% consists of Iran and California recording stations with unknown local site conditions. V_{S30} values are known for more than 85% of stations, on the basis of geophysical investigations at recording sites. The

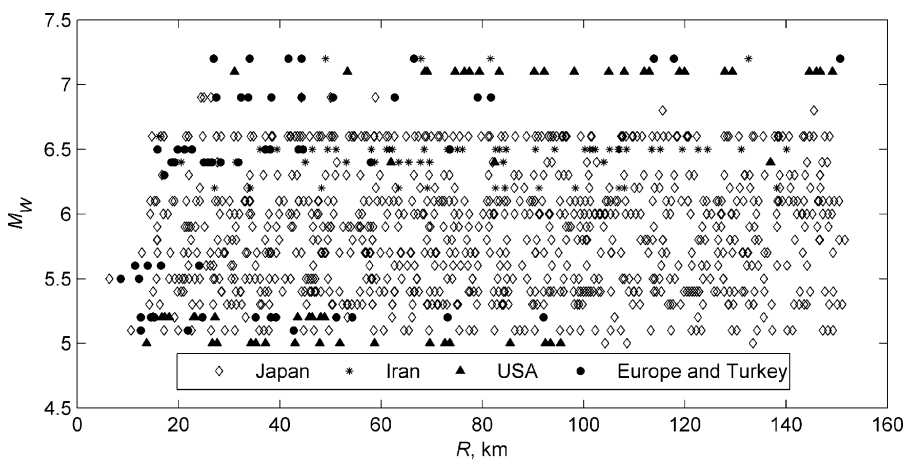

Fig. 1 Distribution of magnitude, distance, and geographical origin for the acceleration records in the database. Note the uniform distribution of data with respect to magnitude and distance

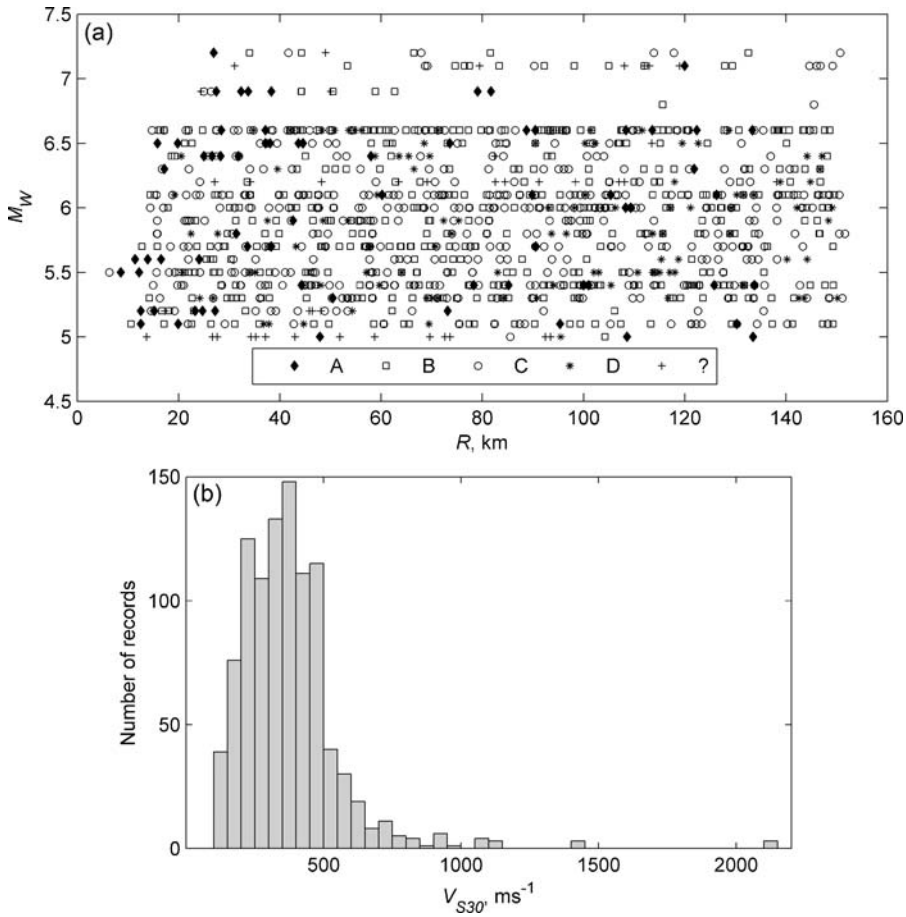

Fig. 2 **a** Distribution of magnitude, distance, and ground category for the records in the database. **b** V_{S30} distribution for the sites of the accelerograph stations in the database

distribution of the available V_{S30} values in the database is depicted in Fig. 2b.

2.5 Dynamic range of the recording instruments

About 90% of the collected data were recorded by accelerometers with a dynamic range exceeding 100 dB. The characteristics of the main types of digital instruments that provided the records in our database are summarized in Table 2.

Note that the simple pre-event baseline correction was sufficient to satisfy the previously mentioned criterion by Paolucci et al. (2008) for 58% of K-Net data, while it proved sufficient only for 22% of Iran data suggesting, as expected, that the resolution of the A/D converter significantly affects the long period noise level in recorded motions. The overall frequency response characteristics of the K-Net accelerographs, which recorded ~83% of the records in the database, is flat from DC to 30 Hz.

2.6 Removal of long period noise and representation of DRS

Based on the previously discussed criterion by Paolucci et al. (2008), the present dataset contains

Table 2 Main types of digital strong motion accelerographs providing records of present database

Instrument type	A/D converter resolution (bit)	Dynamic range (dB)	Region
K-Net95	19	114	Japan
K-Net02	22	132	Japan
SSA-1, SSA-2	12	66	California, Europe, Iran, Turkey
ETNA	18	102	California, Europe
K2	24	138	California, Europe

only spectra associated to a probability $P>0.9$ of long period disturbance levels being less than 15%. Strong-motion records were first processed by the removal of the pre-event offset from the whole time history. By this operation, 57% of our records were brought to satisfy the Paolucci et al. (cit.) criterion. For the remaining records, high-pass filtering of both horizontal components with a T_c=20 s cut-off was applied. This made the noise index small enough to give a probability >90% for the influence of long period noise on the DRS ordinates to be within about 15%. Specifically, we applied fourth-order acausal filters, with cut-off frequency f_c=0.05 Hz, to reduce the influence of the filter cut-off on the usable frequency range of strong motion records (see Boore 2005; Boore and Bommer 2005). Signals were treated by applying cosine taper and zero padding at the beginning and at the end of the time histories. The length of the zero padding depends on the order of the filter and on f_c (Converse and Brady 1992). Note that, according to Akkar and Bommer (2006), a filter corner period of 20 s preserves the response spectral content of the signal *at least* up to 10 s. The DRS ordinates for damping ratios ζ=5%, 10%, 20%, and 30% were computed up to a 20-s period for both horizontal and for the vertical (ζ=5% only) components of each accelerogram, at a period spacing of 0.05 s. The chosen long period limit of 20 s is well beyond the T range needed for displacement-based design of current structures, the *inelastic* vibration periods of which hardly exceed 10 s. The horizontal seismic action is represented in this study by the geometric mean of the DRS ordinates of the two recorded horizontal components at a given period: $\mathrm{DRS}(T;\zeta) = \left[\mathrm{DRS}_x(T;\zeta) \times \mathrm{DRS}_y(T;\zeta)\right]^{1/2}$ and by the single ordinate of the vertical response spectrum. The same definition of the geometric mean is used by Akkar and Bommer (2007a), while Boore and Atkinson (2007, in press) used the so-called GMRotI50 (see Boore et al. 2006), independent of the orientation of the sensors. Boore et al. (cit.) used a large dataset to compare the GMRotI50 with the geometric mean and showed that GMRotI50 is systematically larger, but only by a small amount (less than 3% on average). Campbell and Bozorgnia (2007) made the same comparison for their NGA (PEER 2007) dataset and found the two definitions to differ generally less than 1%. GMRotI50 removes sensor orientation as a contributor to aleatory uncertainty, but this source of variability must be explicitly added back when an estimate of the arbitrary horizontal component is needed.

2.7 Regional dependence of DRS

Following Douglas (2004a, b, 2007), the statistical technique of analysis of variance was used to investigate the possible regional dependence of the displacement response spectra in the database. The purpose of one-way analysis of variance is to find out whether data from several groups have a common mean, i.e., to determine whether the groups differ in the measured characteristic. This aspect is central to the present study, as the necessity to assemble a digital database (see the introduction to the present Section) leads to looking for strong motion records from different geographical regions. Specifically, as digital accelerometer records in Italy and Europe are not enough to ensure a reasonable uniform coverage of the data space, turning to data from other geographical regions (mainly Japan) cannot be avoided. To test the regional dependence of the data, the dataset was subdivided into small intervals (bins) of 10 km×0.3 M_W units, in which an unbalanced one-way analysis of variance was performed. The size of the intervals was chosen so as to ensure the presence of enough records within each bin to perform the analysis. Moreover, only bins with three or more records from each region were considered. Computations were carried out using logarithmically transformed DRS(T;5%) because this transformation is justified by the results of the pure error analysis illustrated in Subsection 3.1. The total number of intervals in which it was possible to perform the analysis is 18 (see Table 3): 2 bins for Europe (E), Japan (J), and California (C); 3 bins for Europe and Japan; 3 bins for California and Japan; 11 bins for Iran (I) and Japan. Within each bin, 400 equally spaced spectral ordinates (from 0.05 to 20 s) were considered. For each spectral ordinate, the null hypothesis H_0 "the median DRS are equal in the regions considered" is rejected if the obtained p value (the smallest level of significance that would lead to rejection of the null hypothesis with the given data) is lower than the chosen significance level α=5%. Results are schematically reported in Table 3 where, for each interval, the geographical origin and the number of observations from each region are speci-

Table 3 Analysis of variance applied by distance–magnitude bins to region of provenance of the data: intervals and results

R (km)	M_W			
	6.5–6.7	6.2–6.4	5.6–5.8	5–5.2
10–19			E(3) J(5) OK	C(5) E(4) J(4) OK
20–29		E(6) J(3)<0.15s		C(6) J(3) OK
30–39	I(4) J(4) OK	I(4) J(4) OK		C(3) E(5) J(5) 10 s–15 s 17 s–20 s
40–49	E(3) J(15) OK			C(7) J(3) OK
60–69	I(7) J(4) <0.45 s	I(7) J(4) 3 s–5.65 s		
70–79	I(3) J(8) <0.2 s			
80–89	I(4) J(6) <0.15 s	I(6) J(6) 3.25 s–7 s		
90–99	I(3) J(18) <0.35 s 2.1 s–8.25 s			C(3) J(4) 0.35 s–1.95 s
100–109	I(9) J(8) <0.8 s 1.2 s–6.6 s; 8.7 s–20 s			
110–119	I(3) J(8) <0.2 s			

The number of observations from each region is specified in parentheses. *E* Europe, *J* Japan, *C* California, *I* Iran, *OK* null hypothesis not rejected

fied. In the present application, the analysis is first carried out without introducing any constraint on site conditions and, subsequently, transforming all the DRS to ground category A, dividing each DRS by the site amplification factor corresponding to the local ground category (see Section 3). This second stage is introduced to check, for those period ranges where regional differences are observed, whether such differences may be related to the presence of different ground categories. Results from the two stages are subsequently combined and the vibration period ranges where the null hypothesis is rejected with both approaches are indicated in Table 3. It turns out that, for α=5%, no strong evidence of regional dependence of DRS can be recognized: for seven bins (labeled with 'OK' in Table 3), there is insufficient evidence to reject H_0 over the whole period range; within all the remaining intervals (with the exception of one, with M_W 6.5–6.7 and R 100–109), the null hypothesis can be rejected only for restricted portions of the investigated period range.

3 Prediction equations

The logical development of our predictive model and the main results obtained by regressing the data are presented in detail in the following subsections, for the 5%-damped horizontal DRS ordinates. The coefficients of the predictive equations for 10%-, 20%- and 30%-damped horizontal DRS are given in Appendix I.xls (provided as Electronic Supplementary Material) for 400 equally spaced values of period between 0.05 s and 20 s, together with the coefficients for the prediction of vertical, 5%-damped DRS. An attenuation relationship for horizontal PGA is also introduced later in the text; the coefficients for different versions of this relationship are given in Appendix I.xls.

3.1 Pure error analysis

Following Douglas and Smit (2001) and Ambraseys et al. (2005), the concept of pure error (Draper and Smith 1981) is used here (1) to establish whether the

standard logarithmic transformation is correct, (2) to investigate the dependence on magnitude of the scatter around the prediction, and (3) to provide the lower bound of the standard deviation (SD) using only magnitude and distance as predictor variables.

To begin with, the logarithmic transformation of the observations (in the present application, the geometric mean of the DRS*(T)* of the two horizontal components) is justified if the errors are proportional to the ground motion amplitude (Draper and Smith, cit.), and it was often used in past studies even though such proportionality was not stated explicitly. To apply the pure error technique, the dataset was subdivided into small bins of 2 km by 0.2 magnitude units, in which the mean (μ) and the unbiased SD of data (σ) was computed via the maximum-likelihood method (Joyner and Boore 1993; Spudich et al. 1999). This can take into account the correlations of data from the same earthquake within each bin. Only bins containing two or more observations were retained for the analysis, the resulting number of cells being 314. The coefficient of variation (COV=$100\sigma/\mu$) was computed and plotted against μ for 400 equally spaced period values from 0.05 s to 20 s: if σ is proportional to μ, these plots should exhibit no significant trend with increasing μ. Hence, a linear equation $\mathrm{COV} = a + b\mu$ was fitted to each graph, and the 95% confidence intervals (CI) of a and b were computed. As the test of size α of the hypothesis H_0: b=0 (H_1: $b\neq 0$) will lead to rejection of H_0 if and only if 0 (zero) is not in the $100(1-\alpha)$% CI of b, use of CIs of b was made and the results showed that, for α=5%, the null hypothesis b=0 cannot be rejected for most periods. Therefore, the logarithmic transformation is justified. Only for T=1.05 and 2.1 s$\leq T\leq$2.7 s, b resulted to be significantly different from zero. However, as for all the neighboring values of T, the logarithmic transformation is justified, it was decided to extend it over the whole period range. A similar choice was made by Ambraseys et al. (cit.).

The dependence of the scatter of the data on magnitude was assessed by plotting σ (recomputed using logarithmically transformed observations) with respect to the mean value of M_W in each bin. For 400 equally spaced periods from 0.05 to 20 s, a linear equation $\sigma = c + dM_W$ was fitted to each data plot, and the 95% confidence intervals of c and d were computed. For all periods, results showed that, for α= 5%, the null hypothesis d=0 cannot be rejected. Therefore, the dependence of the scatter on magnitude can be neglected. Finally, the lower bound of the SD possibly using only magnitude and distance as predictor variables can be assessed. For 400 equally spaced periods from 0.05 to 20 s, the mean SD of the bin SDs was computed. The result showed that the minimum SD of $\log_{10}$ DRS decreases as the vibration period increases, with values roughly varying between 0.34 (for T<1 s) and 0.2 (for T>15 s). The predictive equations for DRS(T) derived herein cannot exhibit standard errors (SE) of the prediction lower than the previous ones, if only magnitude and distance are used as predictor variables.

3.2 On functional forms

Prediction equations characterized by simple functional forms were aimed at, with the minimum number of predictor variables compatible with the information available for the recording sites and the earthquake sources. The simplest reasonable form for such equations was chosen for starting, and complexity was subsequently added in steps, checking the statistical significance of each modification and its influence on the SE of the prediction. The dependent variables of the attenuation relationships are the DRS ordinates from 0.05 to 20 s (though the high-pass filter with f_c=0.05 Hz applied to about 40% of the records may decrease the reliability of the DRS beyond a vibration period of about 15 s) for both the horizontal and the vertical seismic motions. Furthermore, a predictive equation for horizontal peak ground acceleration (PGA) was also obtained.

The empirical equations for the prediction of the DRS*(T;ζ)* ordinates, were initially taken in the form:

$$\begin{aligned}\log_{10}\ \mathrm{DRS}(T;\zeta)(\mathrm{cm}) = {} & a_1 + a_2 M_W \\ & + a_3 \log_{10}\ R(\mathrm{km}) \\ & + a_B S_B + a_C S_C \\ & + a_D S_D + \varepsilon \end{aligned} \qquad (2)$$

where $T(s)$ is the vibration period, ζ is the damping ratio, and a_i (i=1,..D) are numerical coefficients function of period and damping ratio to be determined through regressions. ε denotes a random error term, assumed as normally distributed with zero mean and

SD $\sigma_{\log\ DRS}$. S_B, S_C, S_D are dummy variables accounting for the main ground categories contemplated in the current European Norms (CEN 2004), with the following values: $S_B=S_C=S_D=0$ for type A (rocklike) ground, with $V_{S30}\geq 800$ ms^{-1}; $S_B=1$ and $S_C=S_D=0$ for type B (stiff) ground, with 360 ms$^{-1}\leq V_{S30}<800$ ms^{-1}; $S_B=S_D=0$, $S_C=1$ for type C ground, with 180 ms$^{-1}\leq V_{S30}<360$ ms^{-1}, and $S_B=S_C=0$, $S_D=1$ for type D (very soft) ground, with $V_{S30}<180$ ms^{-1}. Note that accounting for local ground conditions with three dummy variables is strictly necessary to correctly predict the amplification factors with respect to ground type A, especially in terms of range of dominant periods of site response (see Douglas 2003; Faccioli et al. 2007; Pousse et al. 2005). Only a small fraction of accelerograms (less than 4% of the whole database) recorded at sites with unknown ground conditions was retained in the dataset; when regressing the data, these sites were assumed to belong either to class B or to class C, the latter choice providing a slightly lower prediction error. Some tests on the displacement spectral ordinates were performed to investigate whether the statistical significance of the prediction would be increased by adopting a functional form different from Eq. 2. Thus, it was found that the database does not allow to determine both a geometric and dissipative attenuation term (i.e., an additional term a_4R in Eq. 2). By constraining $a_3=-1$ and then determining the inelastic attenuation coefficient a_4 by regression, the results turned out to be statistically significant (for a significance level $\alpha=5\%$) only in the period range 8–12 s, but the decrease in the SE of the prediction was negligible (at most 0.2%). Including a quadratic dependence on M_W leads to statistically significant results only if one sets $a_2=1$ but, again, this brings no significant improvement in the prediction total error (less than 0.4%). We could not calculate from regressions a magnitude-dependent attenuation coefficient a_3, e.g., a decrease of the geometric attenuation factor as magnitude increases. Such a dependence would be more likely detected for $M_W<5.5$ if the lower magnitude bound of the calibration dataset were decreased, e.g., from 5 to 4. In conclusion, no significant improvement was obtained with respect to the results yielded by Eq. 2 that has the additional advantage of allowing in the long period range an immediate comparison with the theoretical attenuation relation for the far field maximum ground displacement derived by Faccioli et al. (2004) from the Brune (1970) model, i.e.:

$$\log_{10}\ d_{\max} = -4.46 + 0.33\log_{10}\Delta\sigma + M_W - \log_{10} R \qquad (3)$$

where $d_{\max}$ (cm) is the maximum ground displacement, $\Delta\sigma$ (MPa) is the stress drop, and R (km) is the focal distance.

3.3 Regression method

The coefficients of the attenuation relationships in this study were computed through a two-stage maximum-likelihood method, as described by Joyner and Boore (1993, 1994). The distance dependence and the site coefficients are determined within the first stage, while the magnitude dependence and the constant term of the predictive equations result from the second step of the regressions. The earthquakes (5 out of 60) associated with a single record in the database are included in the second stage. The component of variability associated with the site is not taken into account. The one-stage maximum-likelihood method (Joyner and Boore 1993) was also tried and then discarded in view of the application within a probabilistic framework because it yielded a slightly higher total SE of the prediction. At an earlier stage (Faccioli et al. 2007), the methods by Joyner and Boore (1981) and Fukushima and Tanaka (1990) were also used, being initially preferred for their easy implementation. The magnitude and distance coefficients for the prediction of DRS(T;5%) are plotted in Fig. 3, as a function of the vibration period T. Note the remarkable agreement at long periods with the theoretical prediction Eq. 3 which, taking a representative value of the stress drop $\Delta\sigma=3$ MPa, yields:

$$\log_{10}\ d_{\max} = -4.3 + M_W - \log_{10}\ R \qquad (4)$$

thus confirming the reliability of the assembled dataset and the soundness of the predictive tool.

3.4 Prediction for rock sites

As shown in Fig. 4, the median spectral shapes predicted by Eq. 2 on ground type A change smoothly

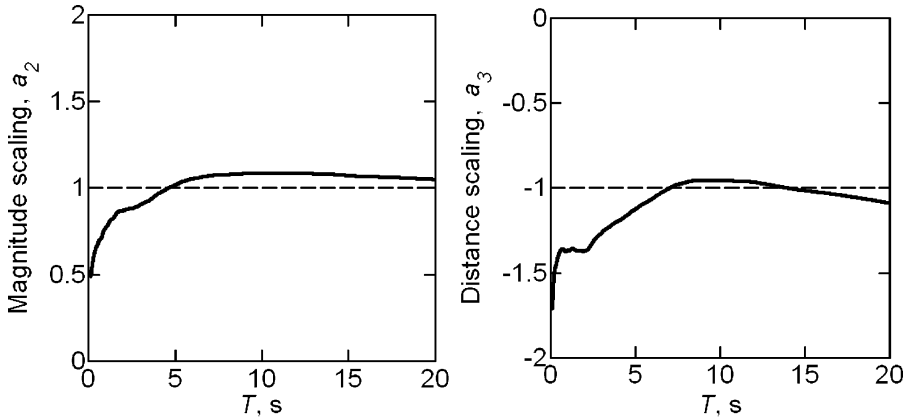

Fig. 3 Dependence on vibration period of the coefficients of magnitude scaling (a_2) and distance scaling (a_3) of observed displacement response spectral ordinates DRS (T;5%), shown by *thick solid curves*. The magnitude and distance dependence of theoretical model (Eq. 4) is also plotted for comparison (*thin dashed lines*)

with M_W and exhibit the same general behavior, i.e., a strongly increasing initial branch up to a "corner" period varying from a few seconds to almost 10 s (depending on magnitude and damping), followed by a branch that smoothly tends to the maximum ground displacement with a nearly constant or moderately decreasing trend.

The spectral ordinates exhibit a tenfold increase for a unit increase in magnitude. Around their maximum value, the 5%-damped DRS are characterized by a "transition" over a period range that becomes wider with magnitude. The median spectral shape smoothly changes with increasing damping as can be appreciated from Fig. 4: the 30%-damped DRS closely approach a bilinear shape. The figure also makes clear that a proper picture of the DRS can be obtained only by considering a very broad period range.

The reduction factor $\eta(T;\zeta)$ of the "overdamped" DRS ordinates with respect to the 5%-damped DRS is shown for ground type A in Fig. 5, where the shaded bands represent the $\pm\sigma$ bounds of the ratios of the median values yielded by Eq. 2, averaged in the distance range 10–50 km. It turns out that the amplitude of $\eta(T;\zeta)$ moderately depends on magnitude and distance, and that the EC8 (CEN 2004) constant reduction factor (dashed lines) seems adequate for periods up to 6–7 s, depending on magnitude. Note that $\eta(T;\zeta) \to 1$ for $T \to 0$ and $T \to \infty$.

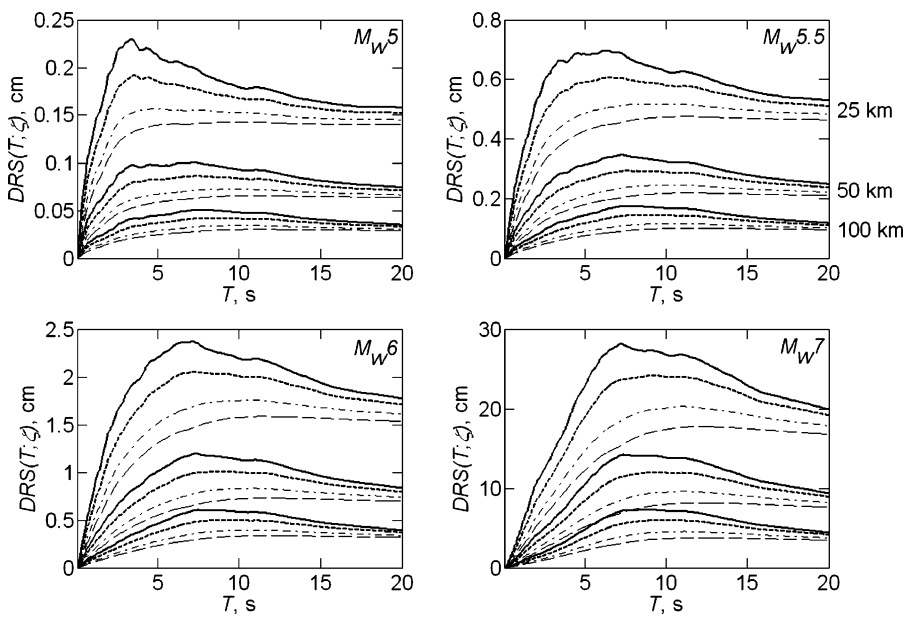

Fig. 4 DRS(T;ζ) predicted on rock by Eq. 2 for different damping ratios: 5% (*thick solid curves*), 10% (*thick dashed curves*), 20% (*thin dot–dashed curves*), 30% (*thin dashed curves*). The spectra are depicted for M_W=5, 5.5, 6, 7 and three values of focal distance R= 25, 50, 100 km

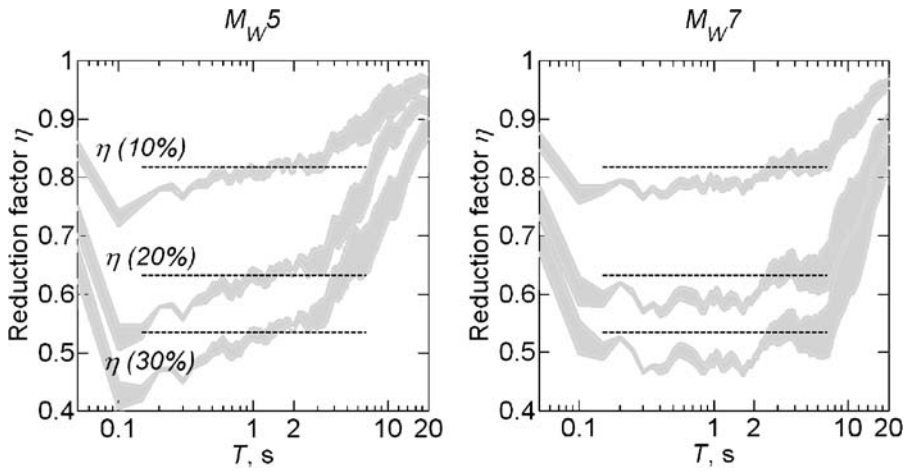

Fig. 5 Reduction factor $\eta(T;\zeta)$ of the overdamped DRS ordinates, averaged in the 10–50 km distance range, with respect to the 5%-damped DRS, ground type A, shown by *shaded bands*. The constant reduction factor contemplated in Eurocode 8 is also shown for comparison (*dashed lines*)

3.5 Influence of style of faulting terms into the equations

The introduction of style of faulting terms into attenuation relationships has been examined in detail by Bommer et al. (2003). While the focal mechanism can be undoubtedly a useful parameter, as the style of rupture of future earthquakes in a particular seismic source zone can usually be defined with some confidence, a number of issues related to the introduction of a further predictor variable has been recognized (see Bommer et al. cit.). Splitting the dataset might affect the robustness of the resulting equations, and differences in ground motions might not be significant enough to justify the incorporation of style of faulting factors into predictive equations; according to some authors, variations attributed to differences in focal mechanism might simply reflect a bias of the data (e.g. Westaway and Smith 1989) and, moreover, comparison with results of different studies is complicated by the use of different classification schemes. With this background, following Boore and Atkinson (2007, in press), we nevertheless investigated the possibility of the source scaling at the second stage of the regressions to take the form:

$$f_S = a_1 + a_2 M_W + a_N E_N + a_R E_R + a_S E_S \qquad (5)$$

where E_x (x=N, R, S) are dummy variables for normal, reverse, and strike-slip fault mechanisms, respectively. Data from all fault types were first grouped together to determine a_1 and a_2. The regressions were then repeated fixing the coefficients a_1 and a_2 to the values obtained when lumping all fault types together and solving for the coefficients a_N, a_R, and a_S of the fault type dummy variables. This leads to constraining the relative scaling of amplitudes with magnitude to be the same for all earthquake types, allowing an offset in the average predicted amplitude level according to the fault mechanism (Boore and Atkinson cit.). The effect of the explicit introduction of a style-of-faulting factor on the total SE of the prediction of 5%-damped DRS was hence examined. It turned out that the introduction of this further variable leads to an appreciable reduction of the total SE of the prediction only in the ranges $T \leq$ 0.2 s and $T \geq 7$ s. Similar investigations were conducted for 10%-, 20%- and 30%-damped DRS. We finally decided to include coefficients for style of faulting in our final model (see Appendix I.xls), but the reader is advised to use them carefully, on the basis of the variation observed in σ with respect to unspecified focal mechanism.

3.6 Influence of site conditions

Particular attention was paid to the assessment of spectral site amplification factors, and it was confirmed that a broad period range must be taken into account for an exhaustive evaluation of site effects on the DRS ordinates. This was actually one of the main motivations for extending our prediction equations to periods lower than 2 s, where the seismic input is normally defined through the acceleration response spectrum in current practice. As discussed in Faccioli et al. (2007), the possible dependence of the ground coefficients a_B, a_C, a_D on magnitude was investigated using a nonlinear predictive relation,

in which a_B, a_C, a_D in Eq. 2 are replaced by $b_4 10^{b_5 M_W}$, $b_6 10^{b_7 M_W}$, $b_8 10^{b_9 M_W}$, respectively. The coefficients obtained for the nonlinear form are not given herein; the results showed that introducing the dependence of site-related coefficients on magnitude leads to a negligible decrease in the SE of the DRS predictions, and the confidence intervals (α=5%) of a_B, a_C, a_D in Eq. 2 cover satisfactorily the amplification factor ranges obtained from the magnitude-dependent form. Nevertheless, this investigation on site terms allowed to detect moderate nonlinear effects in site response, i.e., a decreasing amplification with increasing magnitude for C and D sites.

The availability of the V_{S30} values for about 85% of records in the database allowed us to estimate the site amplification factor as a continuous function of V_{S30}, so as to avoid "jumps" when moving from one ground category to the next. Following Boore et al. (1994, 1997), the site amplification can then be quantified by replacing the terms $a_B S_B + a_C S_C + a_D S_D$ of Eq. 2 as shown in the following equation:

$$\log_{10} \mathrm{DRS}(T;\zeta)(\mathrm{cm}) = a_1 + a_2 M_W + a_3 \log_{10} R(\mathrm{km}) + b_V \log_{10}(V_{S30}/V_a) + \varepsilon \quad (6)$$

b_V and V_a are coefficients that can be estimated through a two-stage weighted regression, in which the dependent variables are the residuals (with respect to the motion predicted by Eq. 2 at rock sites) at those stations where V_S measurements are available. V_a plays the role of a reference shear wave velocity for bedrock and depends on the vibration period T. b_V (negative from the regressions) is also a function of T and exhibits, for ζ=5%, interesting asymptotic properties which can be explained by simple theoretical considerations: at long periods, $|b_V|$ should approach 0.5, as $(V_a/V_{S30})^{0.5}$ is the theoretical site amplification for very smooth V_S variation in sediments. On the other hand, $|b_V|$ should reach 1 in the period range where resonant response of sediments is expected (neglecting the density contrast). The variation of $|b_V|$ and V_a with T is illustrated for ζ=5% in Fig. 6, together with the asymptotic limits just described. As V_a was found to be about 630 ms^{-1} at long periods, for the lower V_{S30} bound of ground category A (V_{S30}= 800 ms^{-1} in Eurocode 8), we faced the problem of ensuring consistency among DRS values obtained from Eqs. 2 and 6. This can be achieved by imposing the additional constraint V_a=800 ms^{-1} (independent of period) in Eq. 6. The influence of local ground type on the spectral response, estimated through different approaches, is depicted in Fig. 7. Here, the 95% confidence intervals of a_B, a_C, a_D in Eq. 2 are compared with the values of the site amplification factor obtained by introducing into Eq. 6 the V_{S30} bounds of the Eurocode 8 ground categories. Note that, by introducing the constraint V_a=800 ms^{-1}, it is no longer possible to clearly segregate the bands of dominant amplification periods of the different

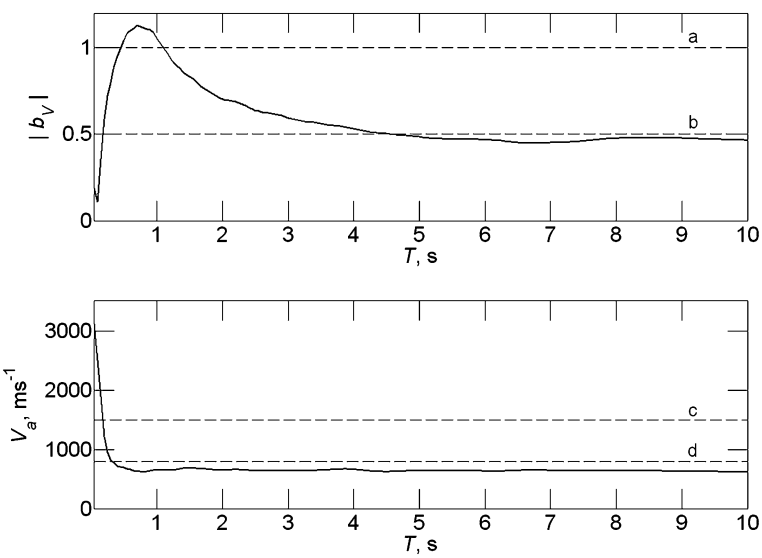

Fig. 6 Variation of the coefficients b_V and V_a of Eq. 6 with period T (*thick black curves*). The thin *horizontal dashed lines* in the *upper graph* denote the theoretical bounds discussed in the text. V_a is approximately 630 ms^{-1} at long periods, lower than both the V_{S30}=800 ms^{-1} bound in Eurocode 8 (curve *d*) and the V_{S30}=1,500 ms^{-1} bound in NEHRP (BSSC 2003) recommendations (curve *c*)

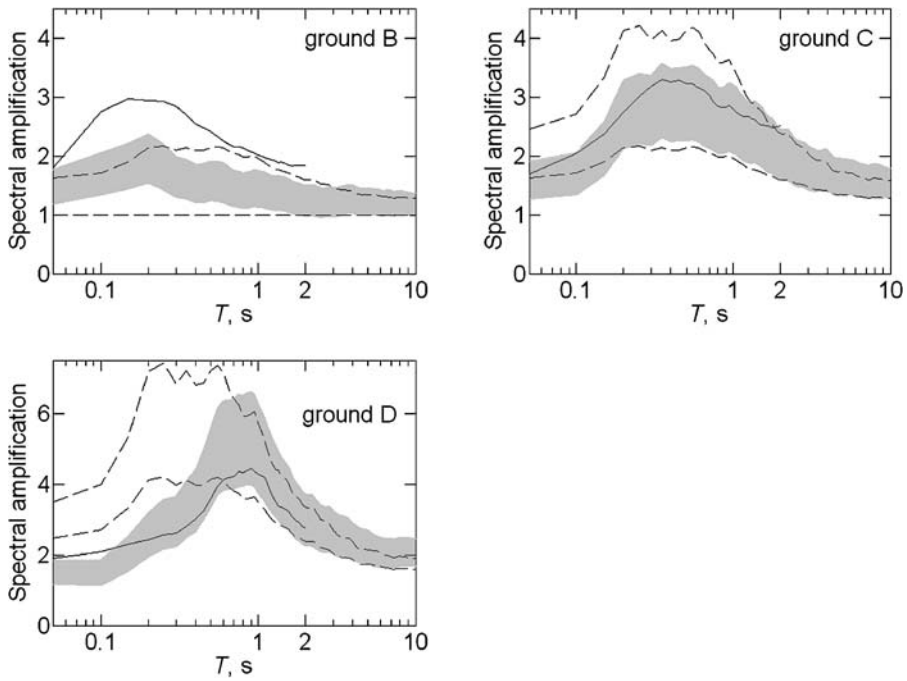

Fig. 7 Spectral amplification curves for ground types B, C, and D. The *shaded bands* depict the 95% confidence intervals of the median values of coefficients a_B, a_C, and a_D in Eq. 2. The *dashed curves* are obtained from the expression $(V_{S30}/V_a)^{b_V}$ by introducing the V_{S30} bounds separating the Eurocode 8 ground categories, i.e., 800 and 360 ms^{-1} for ground type B, 360 and 180 ms^{-1} for ground type C, and 180 and 100 ms^{-1} for type D. The *solid curves* are the average H/V response spectral ratios of observed data for each ground category

ground categories. On the other hand, these period bands are well captured by the mean *H/V r*atios of 5%-damped response spectra, which show a clear site-dependent shape. See Zhao et al. (2006) and Faccioli et al. (2007) for further discussion on this issue.

3.7 Residuals of the DRS predictive equations

The residuals of the predictive equations are computed as the logarithm of the ratio between observed and predicted DRS; two examples are plotted in Fig. 8

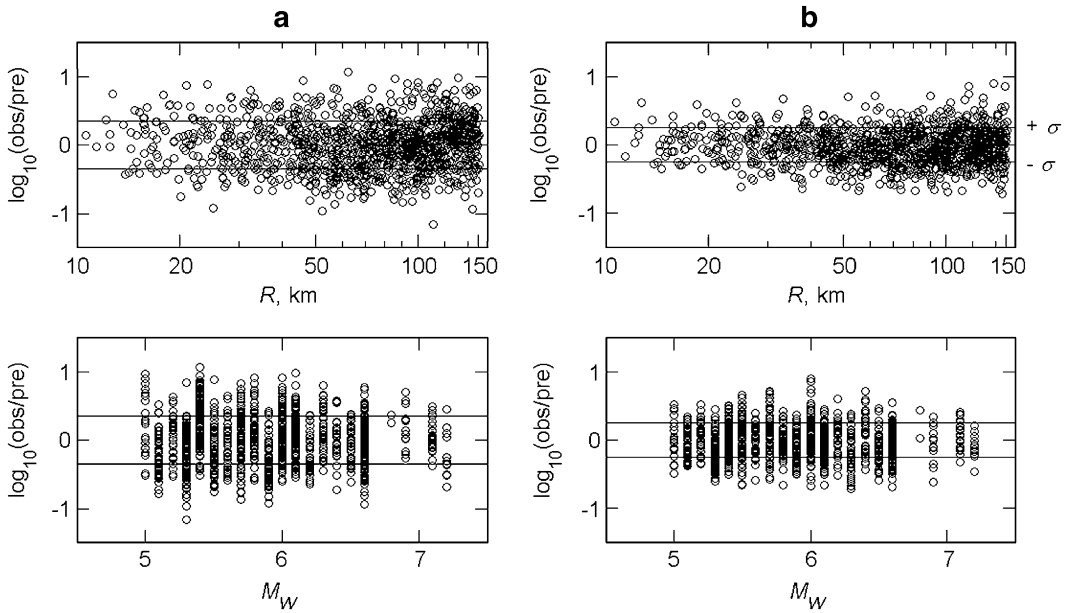

Fig. 8 Residuals of the attenuation relationship at short [T=1 s, (**a**)] and long [T=10 s, (**b**)] period, plotted with respect to magnitude and distance

with respect to the main predictor variables of the attenuation relationship, i.e., moment magnitude M_W and focal distance R. No trend can be recognized, especially at long periods (T=10 s, Fig. 8b), where the dispersion of residuals is small. The SE of the prediction increases as the vibration period decreases, as it appears from the $\pm\sigma$ bands in Fig. 8. This increase in scatter is likely due to the influence of local site amplification associated to ground conditions.

3.8 Tests for earthquakes not included in the dataset

The capability of the present relationships to predict DRS(T) from earthquake records not included in the reference dataset was tested for the M_W 6 Parkfield (California) earthquake, of September 28th, 2004 (focal depth 7.9 km, USGS), by looking at four different T values: 0.5, 1, 5, ad 10 s, and 5%-damped spectra. For simplicity, a functional form analogous to Eq. 2 was adopted, not explicitly containing the site terms, i.e., obtained lumping data from all ground categories together (see Appendix I.xls). The source of Parkfield data is NSMP (including accelerometer records for the Parkfield dense array, Fletcher et al. 1992).

For consistency with the present selection criteria, only the spectra of records having a probability of the long period disturbances less than 15% (with the sole applications of a pre-event baseline correction) were used in the comparison. The chosen focal depth is close to that documented in Fletcher et al. (2006). The results, depicted in Fig. 9, show that the present attenuation relationships can adequately predict the displacement spectral ordinates from earthquakes not included in the database, especially at periods >0.5 s

3.9 Evidence for nonlinear soil response in our database

Nonlinear site amplification as a function of V_{S30} has been examined in depth by Choi and Stewart (2005), who developed empirical relationships for prediction of nonlinear amplification factors for 5%-damped acceleration response spectra, up to 5 s. The results obtained by Choi and Stewart (cit.) were used (with minor modifications and extending the period range up to 10 s) by Boore and Atkinson (2007, in press), while developing their prediction model for pseudo-acceleration spectral ordinates within the NGA Project (PEER 2007). However, Stafford et al.

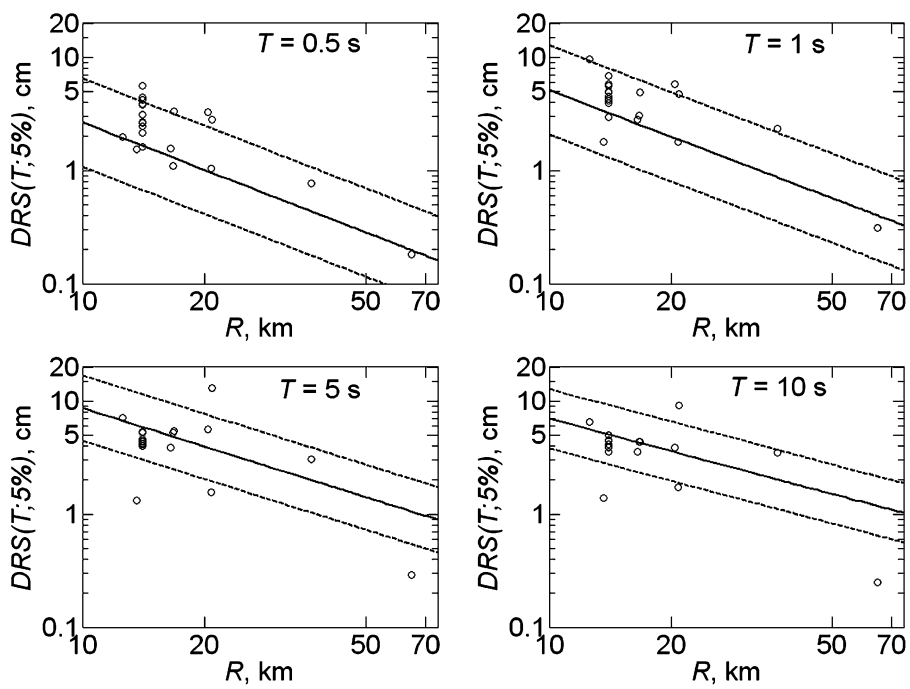

Fig. 9 Ability of present attenuation relationships (shown by *curves* for median ±1 SE values) to predict DRS(T;5%) from earthquakes not included in reference dataset: *symbols* represent observed DRS (5%) ordinates for different values of T from the well recorded M_W 6.0 Parkfield (California) earthquake of September 2004

(2008), while evaluating the applicability of the NGA models to the Euro-Mediterranean region, clearly point out that, though currently available European attenuation relationships do not explicitly model soil nonlinearity, the developers implicitly included ground motions that contains effects associated with such process. Akkar and Bommer (2007b) and Bommer et al. (2007) inspected the distribution of the residuals of their predictive equations, seeking for the evidence of nonlinear soil response. Akkar and Bommer (cit.), though not disputing the existence of soil nonlinearity, did not model it explicitly, as it is not strongly evident in their database. To investigate the possibility of nonlinear response of soil in the present dataset, we inspected the distribution of the residuals of Eq. 2 for 5% damping, as a function of the predicted DRS for ground category B, C, and D, similar to Akkar and Bommer (cit.). The maximum period of interest was set to 3 s, thus focusing on the values of T related to the maximum amplification effects predicted by the present attenuation relationships. Residuals were computed as the common logarithm between the observed and the predicted DRS(T). Thus, a negative trend in the residuals with increasing seismic action would reveal evidence of nonlinear behavior of soils in the database. A significant (α=5%) negative trend was observed only for D sites and 0.45 s≤T≤1.3 s, i.e., the period range where the higher amplification factors are predicted for ground type D. However, if Eq. 6 is used, the negative trend in the residuals is still apparent only for 0.45 s≤T≤0.6 s, T=0.75 s, and T=0.95 s. These results, combined with those on the magnitude dependence of site terms (see Subsection 3.6), show that nonlinear site amplification effects are at most moderate in the database assembled in the present study and, hence, they have not been modeled directly.

3.10 Vertical DRS

The prediction equations for DRS(T;5%) of the vertical component of ground motion have been derived using the same database described in Section 2, reduced to 1,132 records from 60 earthquakes. The coefficients of the attenuation relationships in the form Eq. 2 are listed in Appendix I.xls. The results in terms of the *V/H* ratios of the median vertical 5%-damped spectra and the median horizontal ones, for ground type A and distances ranging between 10 and 50 km, showed that a single simplified envelope appropriate for design application may be used, i.e.,

$$0 \le T \le 0.10 \text{ s}: \quad \mathrm{DRS}_V = \mathrm{DRS}_H \tag{7a}$$

$$0.10\ s < T \le 0.2 \text{ s}: \quad \mathrm{DRS}_V = (4/3 - 10/3 \cdot \mathrm{T})\mathrm{DRS}_H \tag{7b}$$

$$T > 0.2 \text{ s}: \quad \mathrm{DRS}_V = 2/3\mathrm{DRS}_H \tag{7c}$$

where DRS_V is the vertical elastic response spectrum, while DRS_H is the horizontal one. The previous envelope is applicable also to ground categories B, C, and D, although somewhat more conservatively.

4 Comparison with other studies

In this section, a few comparisons are illustrated between the present DRS*(T;5%)* prediction and those based on Akkar and Bommer (2007a) and Boore and Atkinson (2007, in press). As Boore and Atkinson (cit.) predict PSA(T,5%) ordinates, DRS are obtained using the pseudo-spectral relationship. Comparisons are performed following (with slight differences) Campbell and Bozorgnia (2007) who constructed some deterministic earthquake source scenarios with different magnitude and focal mechanism. Deterministic scenarios are used to overcome the complications due to the different distance metric used in the different prediction equations: while the focal distance R is used in the present work, the other authors use the Joyner–Boore distance R_{JB}, i.e., the closest distance from the site to the surface projection of the fault. Figure 10 shows the standard error of prediction of the equations by Boore and Atkinson (cit.), by Akkar and Bommer (cit.) together with that of the present study, for 0.05 s≤T≤10 s. The SE of Boore and Atkinson (cit.) was corrected for the different geometric mean measure of the spectral ordinate, as suggested by Campbell and Bozorgnia (cit.) and converted to the common base 10 logarithm. Note that the total SE obtained herein decreases as the vibration period increases, possibly because of the decrease in scatter induced by site-related amplification effects.

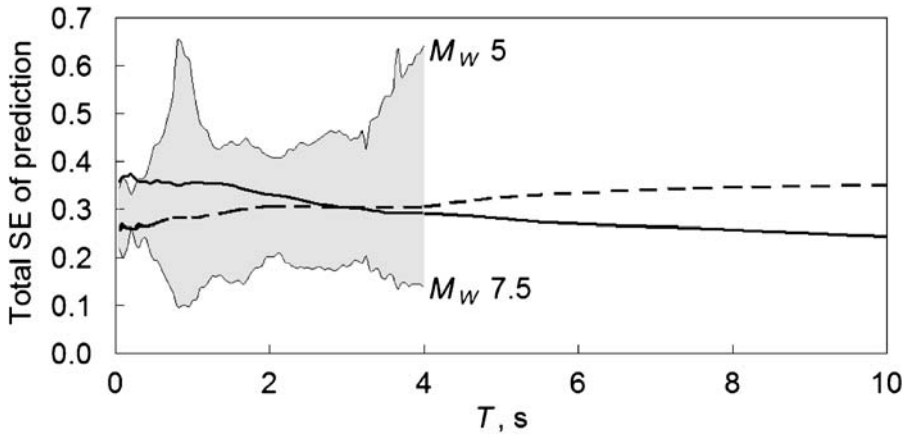

Fig. 10 The standard error (SE) of the prediction equations by Boore and Atkinson (2007, in press), *dashed curve*, compared with that of the present equations, *solid curve*. The SE of Boore and Atkinson was corrected for the different geometric mean measure, as suggested by Campbell and Bozorgnia (2007) and converted to base 10 logarithm. The *shaded band* is the SE of the prediction by Akkar and Bommer (2007a), dependent on magnitude

The deterministic scenarios used are characterized by two values of moment magnitude, M_W 5 and M_W 7. The depth to the top of the coseismic rupture is assumed to be 5 km for the M_W 5 scenario and zero for the M_W 7 one. For the reverse and normal mechanism scenarios, stations are located on the hanging wall of a 45°-dipping fault. The dip of the fault plane of the strike-slip scenario is assumed to be 90°. Stations are located along a line perpendicular to the strike of the fault and passing through the midpoint of the surface projection of the fault The down-dip extent (W) of rupture is computed from rupture area assuming $W = \sqrt{A}$, where the rupture area A is calculated from Wells and Coppersmith (1994). The maximum depth of the seismogenic fault is assumed to be 22 km, consistent with the maximum depth of the events in our database. Comparisons are performed for R_{JB}=10, 25, 50, and 100 km. The corresponding values of R are given in Table 4 for the different scenarios at study. Hypocenters are assumed to be located in the midpoint of the rupture planes, at depths varying between 6 and 11 km. Results are plotted in Fig. 11 for R_{JB}=10 km and R_{JB}=25 km. In Fig. 11, the Eurocode 8 DRS for ground category B are also shown for comparison, with the Type I spectrum used for M_W 7 and the Type II spectrum for M_W5. The Eurocode 8 spectra are anchored to a horizontal reference peak ground acceleration (a_g), which was estimated from the present dataset through Eq. 8 below, using the values of R that correspond to R_{JB}=10 km in Table 4. The style of faulting terms were also used with Eq. 8 (Appendix I.xls). A good agreement can be observed between the median predictions of the different models, confirming the absence of regional dependence of DRS (note that smoothed coefficients are used for the predictions by Akkar and Bommer, cit.). However, for low magnitude earthquakes and long periods, the spectra obtained from Boore and Atkinson (2007, in press) appear less reliable, being heavily influenced by the massive high-pass filtering of the accelerometer records included in their dataset, as it can be appreciated from Fig. 11. For R_{JB}≤25 km and strike-slip events, the predictions of our model for M_W 7 earthquakes, significantly exceed those of the other models.

This effect is, on one hand, related to the values assumed for hypocentral depth in the scenario (generally smaller than the mean depth of the earthquakes in the present database for M_W about 7) and, on the other hand, by the peculiar geometry of the problem.

To cast further light on this point, a further deterministic comparison is presented in Fig. 12 between the present attenuation relationships of those of Akkar and Bommer (2007a), for ζ=5%, two values of magnitude (6 and 7), three values of the Joyner and Boore distance (25, 50, and 100 km), and strike-slip focal mechanism. In the comparison of Fig. 12, we

Table 4 Distance conversions for the deterministic scenarios for strike-slip (S), reverse (R), and normal (N) fault mechanism

R_{JB} (km)	R (km) M_W 5—S	R (km) M_W 5—R	R (km) M_W 5—N	R (km) M_W 7—S	R (km) M_W 7—R	R (km) M_W 7—N
10	11.9	12.6	12.6	14.9	23.7	23.7
25	25.8	26.7	26.7	27.3	37.6	37.6
50	50.4	51.4	51.4	51.2	62	62
100	100.2	101.2	101.2	100.6	111.5	111.5

face the problem of correctly estimating the focal distance values to be used for the comparison, without any knowledge of the fault geometry.

For $M_W \leq 6$, the Joyner and Boore distance can be reasonably taken equal to the epicentral distance: therefore, the focal distance can be obtained using the Joyner and Boore distance and the average depth of our data for $M_W \leq 6$ (equal to ~10 km). For M_W 7, we assumed the fault distance $R_f = \left(R_{JB}^2 + D^2\right)^{0.5}$, where D is average depth of our data for M_W 6.5–7, and computed the focal distance as $R = 0.98R_f + 11.7$, similar to Eq. 1 but obtained using only the strike-slip events of our dataset. After this adjustment, a satisfactory agreement was found, as shown in Fig. 12. This lends further support to the use of a worldwide (predominantly Japanese) database as a basis of ground motion attenuation relationship for a European region, where available digital data are not enough to develop a ground motion prediction model over a broad period range.

The present database was also used to derive an attenuation relationship for horizontal peak ground acceleration, PGA, defined as the geometric mean of the maximum values of the two horizontal compo-

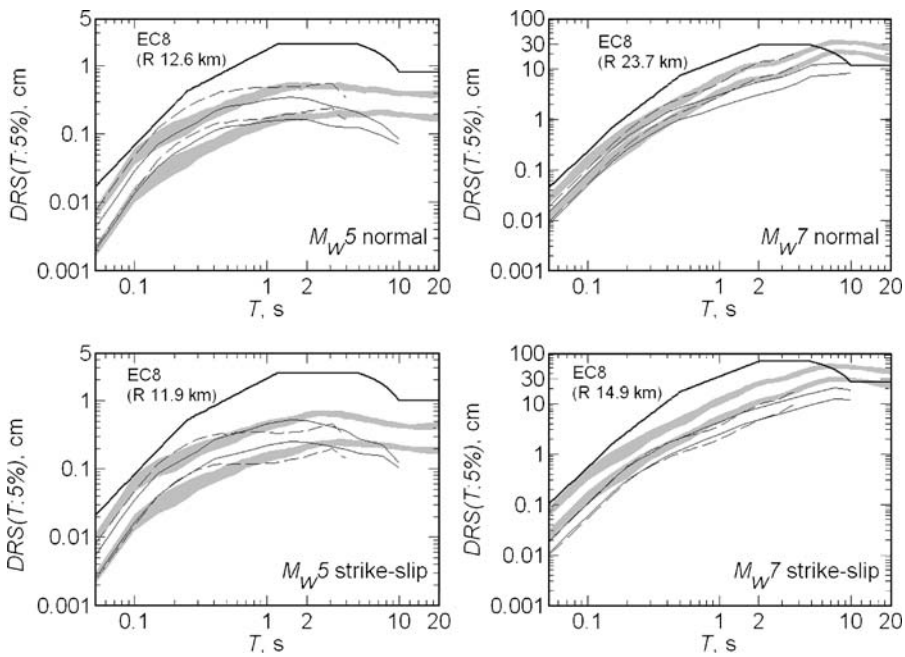

Fig. 11 M_W 5 and M_W 7 comparison scenarios among different DRS(T;5%) predictions. Those resulting from the present work are shown by *shaded bands*, with upper bound given by Eq. 2 for ground category B, and lower bound given by Eq. 6 for V_{S30}=760 and V_a=800 ms^{-1}. *Thin dashed curves* are the spectra yielded by the Akkar and Bommer (2007a) equations, while *thin solid curves* are those from the Boore and Atkinson (2007, in press) equations. Each panel displays two curves for each type of prediction equations, corresponding to values of the Joyner and Boore distance, R_{JB}, equal to 10 and 25 km. The Eurocode 8 (EC8) displacement spectra for ground category B are also shown for comparison, by *thick solid curves*. The EC8 spectra are anchored to a reference horizontal peak ground acceleration estimated from Eq. 8, using the style of faulting factors listed in Appendix I.xls and the indicated magnitude and distance values. EC8 types II and I spectra were used for M_W 5 and M_W 7, respectively

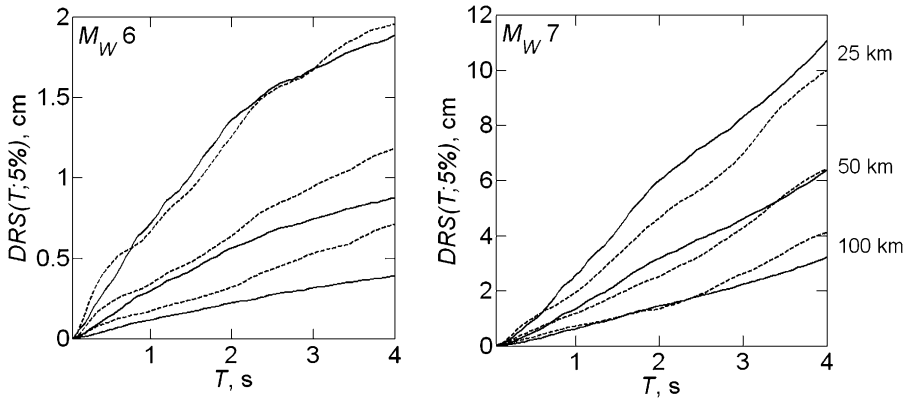

Fig. 12 Comparison between spectra predicted by the present DRS attenuation relationships (*solid curves*) and those derived by Akkar and Bommer (2007a) using data from Europe and the Middle East (*dashed curves*). The spectra are plotted for three values of the Joyner–Boore distance (25, 50, and 100 km), for ζ=5% and strike-slip style of faulting. Note the remarkable agreement between the two attenuation relationships suggesting no evidence of regional dependence of DRS

nents, i.e., $\mathrm{PGA} = \left(\mathrm{PGA}_x \times \mathrm{PGA}_y\right)^{1/2}$. The simplest functional form for the prediction of the PGA was found to be:

$$\begin{aligned}\log_{10}\mathrm{PGA}\left(\mathrm{ms}^{-2}\right) &= -1.296 + 0.556M_W \\ &\quad - 1.582\log_{10}R(\mathrm{km}) \\ &\quad + 0.22S_B + 0.304S_C \\ &\quad + 0.332S_D \pm 0.344 \end{aligned} \tag{8}$$

while the coefficients of the attenuation model including the style of faulting factor and site terms as a function of V_{S30} are given in Appendix I.xls. Eq. 8 is compared in Fig. 13, for rock sites and strike-slip fault mechanism, with the relationships by Ambraseys et al. (2005) and Akkar and Bommer (2007a), who used data from Europe and the Middle East. The focal distance used in our equation was estimated as described in the previous paragraph. Note that the Ambraseys et al. (2005) response variable is the larger horizontal component of the ground motion. While a good agreement is found among the predictive models for M_W 6 and 7, the comparison is less satisfactory for M_W 5, where Eq. 8 gives lower median predictions over the whole distance range considered. Nevertheless, the median values of Ambraseys et al. (cit.) and Akkar and Bommer (cit.) are within the SE bounds of our prediction also for M_W 5. The noted difference is related to the fairly high magnitude scaling coefficient in Eq. 8, mostly influenced by the chosen upper bound M_W 7.2 in the present dataset, compared with values of 7.6 used by Ambraseys et al. (cit.) and Akkar and Bommer (cit.). The same difference in the M_W upper bound is also likely to be the main cause for the high distance decay coefficient in Eq. 8 because the observed rate of attenuation of peak accelerations

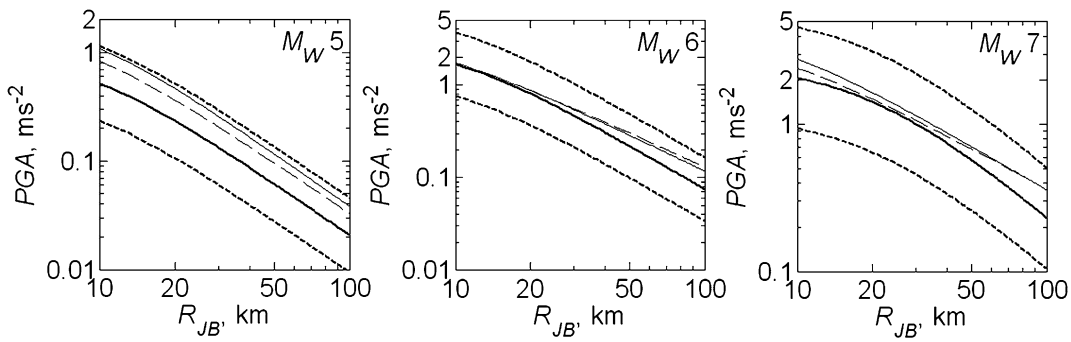

Fig. 13 Comparison between the attenuation relationship for PGA calibrated in the present study (*thick curves*, median values ±1 SE) and that developed by Ambraseys et al. (2005), *thin solid curves*, and Akkar and Bommer (2007a), *thin dashed curves*, for rocklike sites and strike-slip mechanism

with distance tends to decrease at the higher magnitudes (see, e.g., Ambraseys et al., cit.).

5 Discussion and conclusions

Using a fully digital accelerometer database, a new set of equations for empirical prediction of arbitrarily damped horizontal DRS(T) ordinates from 20 Hz to 20 s has been derived, together with prediction models for 5%-damped vertical DRS(T) and PGA. Thanks to the application of a very recent method (Paolucci et al. 2008) to assess the long period reliability of the DRS(T), the same number of records of the full database could be used for the calibration over the entire range of vibration periods from 0.05 to 20 s. At long periods, the results are consistent with the theoretical attenuation relationship by Faccioli et al. (2004). The use of analysis of variance and the deterministic comparisons with other recent studies in Europe and in the United States show that the evidence of regional dependence of the DRS(T) ordinates is very weak. These results lend strong support to the use of worldwide data, predominantly from Japan, to derive DRS attenuation relationship for a European region, such as Italy, where the available digital data are not enough to develop a reliable prediction model over a broad period range.

The careful treatment devoted to the study of site-related amplification effects has resulted in a prediction model capable of segregating the dominant periods of site response for the main ground categories contemplated in the Eurocode 8 (CEN 2004). Moreover, the alternative use of V_{S30} as predictor variable allows to estimate the spectral site amplification as a continuous function of the mechanical properties of the foundation soils.

The displacement response spectra recommended by Eurocode 8 have been compared in Fig. 11, for assigned magnitudes and distances, with the spectra predicted by the proposed equations as well as by other recent ones. The code spectra appear to significantly overestimate the empirical predictions over a broad period range, notably for $T>0.3$ s. The difference is especially notable at the lower magnitudes, where the Type II Eurocode spectra apply. At large magnitude, where the Type I spectra apply, there is reasonable agreement at very long periods (5 s$<T<$ 10 s). It is hoped that the noted differences will stimulate some adjustments in the Eurocode 8 spectra in the near future.

In the aim of checking the limits of applicability of the present attenuation equations, we have also used the accelerograms from a number of well-recorded earthquakes from the present dataset to derive velocity spectral response values. We then compared such spectra with the pseudo-velocity (PSV) ordinates obtained form the relationship $\mathrm{PSV}(T) = (2\pi/T)\mathrm{DRS}(T)$. The ratio SV/PSV was found to remain approximately constant, with values between 1.1 and 1.5, within a limited range of periods, namely, 0.2–1.0 s for M_W 5 and 0.2–7 s for M_W 7. Hence, the PSV spectra derived from the present DRS predictions cannot be regarded as reliable estimates of the true velocity spectra. Further aspects of this topic have been discussed, e.g., by Jangid and Kelly (2001). On the other hand, we found acceleration (SA) and pseudo-acceleration (PSA) spectra to be essentially coincident from 0.05 to at least a 10-s period.

The empirical equation calibrated within this study can be easily implemented into a computer program for seismic hazard assessment, being characterized by a simple functional form and a restricted number of predictor variables. Moreover, the application of the present attenuation relationships can easily lead to a simplified model of the seismic action in terms of DRS(T) apt for introduction in seismic codes.

Acknowledgments This work has been mostly carried out in the framework of the Italian seismological project S5 (*Definizione dell'input sismico sulla base degli spostamenti attesi*) of the 2006-07 DPC-INGV research programs. While all the sources of our data are gratefully acknowledged, a special mention is devoted to the managing authorities and the maintainers of the Japanese K-Net, Kik-Net, and F-Net for making such a wealth of very good quality data available to the scientific community. The Kobe data used here were collected and distributed by the Japanese Working Group on Effects of Surface Geology on Seismic Motion, Association for Earthquake Disaster Prevention, for the Kobe Simultaneous Simulation Project during the second International Symposium on Effect of Surface Geology on Strong Motions (ESG98) held at Yokohama, Japan, in 1998. The contribution of R. Paolucci, especially in investigating the correction procedures for digital accelerograms, is gratefully acknowledged. We are grateful to J. Douglas and an anonymous reviewer for their remarks and suggestions, which helped us significantly in improving the manuscript.

References

Akkar S, Bommer JJ (2006) Influence of long-period filter cut-off on elastic spectral displacements. Earthquake Eng Struct Dyn 35:1145–1165

Akkar S, Bommer JJ (2007a) Prediction of elastic displacement response spectra in Europe and the Middle East. Earthquake Eng Struct Dyn 36(10):1275–1301

Akkar S, Bommer JJ (2007b) Empirical prediction equations for peak ground velocity derived from strong-motion records from Europe and the Middle East. Bull Seism Soc Am 97(2):511–530

Ambraseys N, Smit P, Sigbjornsson R, Suhadolc P, Margaris B (2002) Internet-site for European strong-motion data. European Commission, Research-Directorate General, Environment and Climate Programme, www.isesd.cv.ic.ac.uk/ESD

Ambraseys NN, Douglas J, Sarma SK, Smit PM (2005) Equations for the estimation of strong ground motions from shallow crustal earthquakes using data from Europe and the Middle East: horizontal peak ground acceleration and spectral acceleration. Bull Earthq Eng 3:1–53

Berge-Thierry C, Cotton F, Scotti O, Griot-Pomniera DA, Fukushima Y (2003) New empirical spectral response attenuation laws for moderate European earthquakes. J Earthq Eng 7(2):193–222

Bommer JJ, Douglas J, Strasser FO (2003) Style-of-faulting in ground-motion prediction equations. Bull Earthq Eng 1:171–203

Bommer JJ, Stafford PJ, Alarcón JE, Akkar S (2007) The influence of magnitude range on empirical ground-motion prediction. Bull Seism Soc Am 97(6):2152–2170

Boore DM (2001) Effect of baseline corrections on displacements and response spectra for several recordings of the 1999 Chi-Chi, Taiwan, earthquake. Bull Seismol Soc Am 91 (5):1199–1211

Boore DM (2004) Estimating $V_S(30)$ (or NEHRP site classes) from shallow velocity models (depths <30 m). Bull Seismol Soc Am 94(2):591–597

Boore DM (2005) On pads and filters: processing strong-motion data. Bull Seismol Soc Am 95(2):745–750

Boore DM, Joyner WB, Fumal TE (1994) Estimation of response spectra and peak accelerations from Western North American earthquakes: an interim report—part 2. USGS open-file report 94–127

Boore DM, Joyner WB, Fumal TE (1997) Equations for estimating horizontal response spectra and peak acceleration from Western North American earthquakes: a summary of recent work. Seismol Res Lett 68(1):128–153

Boore DM, Stephens CD, Joyner WB (2002) Comment on baseline correction of digital strong-motion data: examples from the 1999 Hector Mine, California, earthquake. Bull Seismol Soc Am 92(4):1543–1560

Boore DM, Bommer JJ (2005) Processing of strong-motion accelerograms: needs, options and consequences. Soil Dyn Earthqu Eng 25(2005):93–115

Boore DM, Watson-Lamprey J, Abrahamson NA (2006) GMRotD and GMRotI: orientation-independent measures of ground motion. Bull Seismol Soc Am 96:1502–1511

Boore DM, Atkinson GM (2007) Boore-Atkinson NGA ground motion relations for the geometric mean horizontal component of peak and spectral ground motion parameters, PEER 2007/01, Pacific Earthquake Engineering Research Center, Berkeley, California

Boore DM, Atkinson GM (in press) Ground-motion prediction equations for the average horizontal component of PGA, PGV, and 5%-damped PSA at spectral periods between 0.01 s and 10.0 s. Earthq Spectra

Brune JN (1970) Tectonic stress and the spectra of seismic shear waves. J Geophys Res 75:4997–5009

BSSC, Building Seismic Safety Council (2003) The 2003 NEHRP Recommended provisions for new buildings and other structures. Part 1: provisions (FEMA 450), www.bssconline.org

Campbell KW, Bozorgnia Y (2007) Campbell-Bozorgnia NGA ground motion relations for the geometric mean horizontal component of peak and spectral ground motion parameters, PEER 2007/02, Pacific Earthquake Engineering Research Center, Berkeley, California

CEN, European Committee for Standardization (2004) Eurocode 8: design of structures for earthquake resistance—part 1: general rules, seismic actions and rules for buildings. Bruxelles

Choi Y, Stewart JP (2005) Nonlinear site amplification as a function of 30 m shear wave velocity. Earthq Spectra 21(1):1–30

Converse AM, Brady AG (1992) BAP: basic strong-motion accelerogram processing software, version 1.0. USGS Open-File Rept. 92-296A, 174 pp

Douglas J (2003) Earthquake ground motion estimation using strong-motion records: a review of the equations for the estimation of peak ground acceleration and response spectral ordinates. Earth-Sci Rev 61:43–104

Douglas J (2004a) An investigation of analysis of variance as a tool for exploring regional differences in strong ground motions. J Seismol 8:485–496

Douglas J (2004b) Use of analysis of variance as a tool for the investigation of regional dependence of strong ground motions. In: Proceedings of the13th World Conference on Earthquake Engineering, Vancouver, B. C., Canada, Paper no. 29

Douglas J (2007) On the regional dependence of earthquake response spectra. ISET J Earthq Technol 44(1):71–99

Douglas J, Smit PM (2001) How accurate can strong ground motion attenuation relations be? Bull Seismol Soc Am 91 (6):1917–1923

Draper NR, Smith H (1981) Applied regression analysis, 2nd edn. Wiley, New York

Faccioli E, Paolucci R, Rey J (2004) Displacement spectra for long periods. Earthq Spectra 20:347–376

Faccioli E, Cauzzi C, Paolucci R, Vanini M, Villani M, Finazzi D (2007) Long period strong ground motion and its use as input to displacement based design. In: Pitilakis K (ed) Earthquake geotechnical engineering. 4th International Conference on Earthquake Geotechnical Engineering—Invited Lectures. Springer Netherlands

Figini R (2006) Analisi degli effetti di sito sui lunghi periodi degli spettri di risposta di spostamento. Master's Thesis, Politecnico di Milano

Fletcher JB, Baker LM, Spudich P, Goldstein P, Sims JD, Hellweg M (1992) The USGS Parkfield, California, dense seismograph array: UPSAR. Bull Seismol Soc Am 82:1041–1070

Fletcher JB, Spudich P, Baker LM (2006) Rupture propagation of the 2004 Parkfield, California, earthquake from observations at UPSAR. Bull Seismol Soc Am 96(4B): S129–S142

Fukushima Y, Tanaka T (1990) A new attenuation relation for peak horizontal acceleration of strong earthquake ground motion in Japan. Bull Seismol Soc Am 80(4): 757–783

Gruppo di lavoro CPTI (2004) Catalogo Parametrico dei Terremoti Italiani, versione 2004 (CPTI04). Istituto Nazionale di Geofisica e Vulcanologia (INGV), Bologna, emidius.mi.ingv.it/CPTI

Halldórsson B, Ólafsson S, Sigbjörnsson R (2007) A fast and efficient simulation of the far-fault and near-fault earthquake ground motions associated with the June 17 and 21, 2000, earthquakes in South Iceland. J Earthq Eng 11:343–370

Jangid RS, Kelly JM (2001) Base isolation for near-fault motions. Earthquake Eng Struct Dyn 30(5):691–707

Japanese Working Group on Effects of Surface Geology on Seismic Motion, Association for Earthquake Disaster Prevention (1998) CD-ROM for the Kobe simultaneous simulation, distributed to participants to the experiment. Proc. of the 2nd International Symposium on the Effects of Surface Geology on Earthquake Ground Motion, Yokohama, Japan

Jousset P, Douglas J (2007) Long-period earthquake ground displacements recorded on Guadeloupe (French Antilles). Earthquake Eng Struct Dyn 36(7):949–963

Joyner WB, Boore DM (1981) Peak horizontal acceleration and velocity from strong-motion records including records from the 1979 Imperial Valley, California, earthquake. Bull Seismol Soc Am 71(6):2011–2038

Joyner WB, Boore DM (1993) Methods for regression analysis of strong-motion data. Bull Seismol Soc Am 83(2):469–487

Joyner WB, Boore DM (1994) Errata: methods for regression analysis of strong-motion data. Bull Seismol Soc Am 84:955–956

Paolucci R, Rovelli A, Faccioli E, Cauzzi C, Finazzi D, Vanini M, Di Alessandro C, Calderoni G (2008) On the reliability of long period spectral ordinates from digital accelerograms. Earthquake Engng Struct Dyn 2008(37):697–710

Park R, Paulay T (1976) Reinforced concrete structures. Wiley, New York

PEER, Pacific Earthquake Engineering Research Center (2007) Next generation attenuation of ground motions (NGA) project. Web site: peer.berkeley.edu/products/nga_project.html

Pousse G, Berge-Thierry C, Bonilla F, Bard PY (2005) Eurocode 8 design response spectra evaluation using the K-Net Japanese database. J Earthq Eng 9(4):547–574

Priestley MJN, Calvi GM, Kowalsky MJ (2007) Displacement-based seismic design of structures. IUSS, Pavia

Rathje EM, Stewart JP, Bora Baturay M, Bray JD, Bardet JP (2006) Strong ground motions and damage patterns from the 1999 Duzce earthquake in Turkey. J Earthq Eng 10(5):693–724

Rey J, Faccioli E, Bommer J (2002) Derivation of design soil coefficients (S) and response spectral shapes for Eurocode 8 using the European strong motion database. J Seismol 6 (4):547–555

Spudich P, Joyner WB, Lindh AG, Boore DM, Margaris DM, Fletcher JB (1999) SEA99: a revised ground motion prediction relation for use in extensional tectonic regimes. Bull Seismol Soc Am 89(5):1156–1170

Stafford PJ, Strasser FO, Bommer JJ (2008) An evaluation of the applicability of the NGA models to ground-motion prediction in the Euro-Mediterranean Region. Bull Earthq Eng DOI 10.1007/s10518-007-9053-2

Wang GQ, Boore DM, Tang G, Zhou X (2007) Comparisons of ground motions from colocated and closely spaced one-sample-per-second global positioning system and accelerograph recordings of the 2003 M 6.5 San Simeon, California, earthquake in the Parkfield region. Bull Seismol Soc Am 97 (1B):76–90

Wells DL, Coppersmith KJ (1994) New empirical relationships among magnitude, rupture length, rupture width, rupture area, and surface displacement. Bull Seismol Soc Am 84:974–1002

Westaway R, Smith RB (1989) Strong ground motion in normal-faulting earthquakes. Geophys J 96:529–559

Zaré M (2004) Long period Iranian strong motions recorded during 1994–2002, processing and analysis. In: Proceedings of the13th World Conference on Earthquake Engineering, Vancouver, B. C., Canada, Paper no. 2002

Zhao JX, Irikura K, Zhang J, Fukushima Y, Somerville PG, Asano A, Ohno Y, Oouchi T, Takahashi T, Ogawa H (2006) An empirical site-classification method for strong-motion stations in Japan using H/V response spectral ratio. Bull Seismol Soc Am 96:914–925